Study on Erosion Characteristics and Mechanisms of Recycled Concrete with Tailings in Salt Spray Environments

Jin Xu [1,2,3], Tao Li [4,5,*], Meng Zhan [4], Xiuyun Chen [4], Fan Xu [6] and Sheliang Wang [3]

1 School of Civil Engineering, Xijing University, Xi'an 710123, China; 20160030@xijing.edu.cn
2 Shaanxi Key Laboratory of Safety and Durability of Concrete Structure, Xi'an 710123, China
3 School of Civil Engineering, Xi'an University of Architecture and Technology, Xi'an 710055, China; sheliangw@163.com
4 College of Architecture Engineering, Huanghuai University, Zhumadian 463000, China; zhanyi313@163.com (M.Z.); chenxiuyun@huanghuai.edu.cn (X.C.)
5 College of Urban, Rural Planning and Architectural Engineering, Shangluo University, Shangluo 726000, China
6 School of Civil and Architecture Engineering, Xi'an Technological University, Xi'an 710021, China; xufanxf1205@163.com
* Correspondence: litao623114@126.com

Abstract: To improve the utilization efficiency of iron tailings (IOT) and recycled coarse aggregate (RCA), the mechanical properties, erosion depth and other erosion characteristics of recycled aggregate concrete (RAC) with different IOT amounts were studied in salt spray erosion environments and the erosion mechanisms were analyzed by SEM technology. The results showed that at the same erosion age, IOT caused the compressive strength and splitting tensile strength of RAC to tend to first increase and then decrease, with the optimum mixing amount being approximately 40%. Under the same conditions, the erosion depth of RAC was much higher than that of ordinary concrete. The erosion depth first decreased and then increased with an increasing amount of IOT. When the IOT content was 30–40%, the salt spray erosion depth reached its minimum. The solidification coefficient K_1 first decreased and then increased with the increase in iron tailings content. At its lowest point, the iron tailings content was approximately between 30% and 50%, which demonstrated that the higher the salt spray erosion age, the larger the solidification coefficient. Through SEM microscopic images, it could be seen that the appropriate amount of iron tailings caused the formation of salt spray erosion crystals and that the effect of physical expansion pressure caused a reduction in the porosity of RAC and a slight increase in its mechanical properties and salt spray erosion resistance. When the iron tailings content was large, the optimal mix ratio of the concrete also changed and then harmful pores and cracks were regenerated. Therefore, resistance to salt spray erosion was weakened. The research in this paper provides a theoretical basis for the engineering application of recycled concrete with tailings in salt spray environments.

Keywords: iron tailings; recycled concrete; salt spray environment; erosion characteristics; erosion mechanisms

1. Introduction

As granular waste from iron ore smelting, IOT have the obvious characteristics of fine powder and pozzolanic activation [1]. The porosity and related mechanical properties of recycled aggregate concrete are lower than those of ordinary concrete due to the existence of adhesive mortar [2,3]. At the same time, the utilization rate of IOT in China is less than 30%, which is far lower than the 90% rates in other developed countries [4,5]. Finally, a large amount of funds needs to be invested every year to deal with this problem, which has become the main factor in the restriction of the economic and ecological development of our country. When we are able to give full play to the respective performance of IOT

and combine them with RAC to make recycled concrete with tailings, it improves their performance and provides a strong push to respond to the national policy of "clear waters and green mountains are as good as mountains of gold and silver".

Under the action of salt spray, chloride ions that attach to the concrete surface gradually erode and soak into the concrete, resulting in the destruction of the passive film of the reinforcement, the erosion of the reinforcement and even the durability failure of the structure [6]. Kamiharako [7] analyzed the relationship between the number of chloride ions attached to a structure's surface and the shape of the structure through numerical simulation and software analysis. Then, a set of techniques were proposed for applying these results to the prediction of the amount of chloride ingress in the concrete members of a bridge superstructure. Chendra [8] analyzed the main influencing factor of flow field on the chloride ion adsorption capacity of a concrete surface by using the wind tunnel test. Then, the amount of sea salt in the air was estimated through numerical simulation (computational fluid dynamics). Mohamed [9] developed a new artificial neural network (ANN) to predict the chloride ion penetration level and compressive strength of a self-compacting concrete mixture, which was in good agreement with our test results. Ariyachandra [10] discussed the effect of NO_2 isolated recycled concrete aggregate (NRCA) on the chloride diffusion and chloride binding capacity of concrete, the results of which showed that the addition of NRCA increased the formation of Friedel's salt and Kuzel's salt in concrete and enhanced the chloride ion binding ability of concrete. The results also identified the mechanisms for enhancing the chloride ion erosion resistance of NRCA mixed concrete. Rajamallu [11] studied the chloride ion permeability and erosion characteristics of cement concrete that was partially replaced by slag and silica fume and showed that it could strengthen erosion resistance. Su [12] simulated the combined effects of marine salt spray environments and fatigue alternating loads. The results showed that the greater the stress level and the greater the loading frequency, the greater the chloride ion content at the same depth.

At present, experts and scholars have systematically studied the erosion characteristics and erosion mechanisms of ordinary concrete in salt spray environments, but research on recycled concrete with iron tailings has been relatively less extensive. Oritola [13] used microscopic and physical examination techniques to test and evaluate five types of iron tailings that were obtained from different places and compared them to ordinary natural aggregate. The results showed that iron tailings could be used well in concrete. Protasio [14] studied the pozzolanic activity and comprehensive pore size distribution of concrete with iron tailings using thermogravimetric analysis, XRD and uniaxial compression tests. Then, the influence laws of different replacement proportions of iron tailings on the compressive strength and workability of concrete were obtained. Wang [15] studied the strength of recycled concrete that was mixed with construction waste and iron tailings. When the additional water content of the recycled aggregate was 0% and the content of iron tailings was 60%, the compressive strength of the recycled concrete was at its highest. Wei [16] conducted experimental research on 12 groups of high-ductility recycled concrete with iron tailings and systematically studied the main mechanical properties, such as compressive strength, flexural strength and splitting tensile strength. The results showed that the mechanical properties first increased and then decreased with the increase in iron tailings content and reached a peak when the iron tailings content was 30%. Cui [17] used the variance analysis method to analyze the compressive strength of recycled concrete with iron tailings under different working conditions. Professor Wang of the Xi'an University of Architecture and Technology [18–22] conducted a systematic macro- and micro-analysis on the strength, mechanical properties, deformation properties, carbonation, freeze–thaw cycles and other durability factors of recycled concrete with tailings, which provided a valuable basis for the development of recycled concrete with tailings.

Therefore, this paper studied the erosion characteristics and mechanisms of recycled concrete with different amounts of iron tailings under different periods of salt spray erosion

in order to find the optimal amount of iron tailings for salt spray environments and provide a theoretical basis for engineering applications.

2. Test Materials

Qinling ordinary portland cement (p.o.42.5) and Bahe natural river sand were used in our tests. Natural coarse aggregate (NCA) was made from artificial crushed stone with particle size range of 5–20 mm and continuous grading. Recycled coarse aggregate (RCA) was a common material found in Xi'an market, which has been in service for 30 years. The strength grade of the original concrete was C30. After screening, cleaning, drying, bagging and the other procedures, it could be used for later tests.

The iron tailings (IOT) came from the YAOGOU tailings reservoir in Shangluo, Shaanxi Province, which was accumulated by the waste slag that was generated after steelmaking and covered an area of nearly 1000 square meters up to 6.8 m high. According to incomplete statistics, the accumulation of tailings accounted for 45.67% of industrial waste in China. In 2020–2021, the comprehensive utilization of industrial solid waste was 2.059 billion tons with a utilization rate of 62.3%, but this rate for tailings was only 18.9%, which still leaves a lot of room for development. In this paper, the constituent elements of iron tailings were determined using energy spectrum analysis with the Vario EL cube and the particle gradation was determined using a negative pressure grading screen, as shown in Figure 1, Tables 1–3. The performances of the main test materials met the requirements for the relevant specifications [23,24].
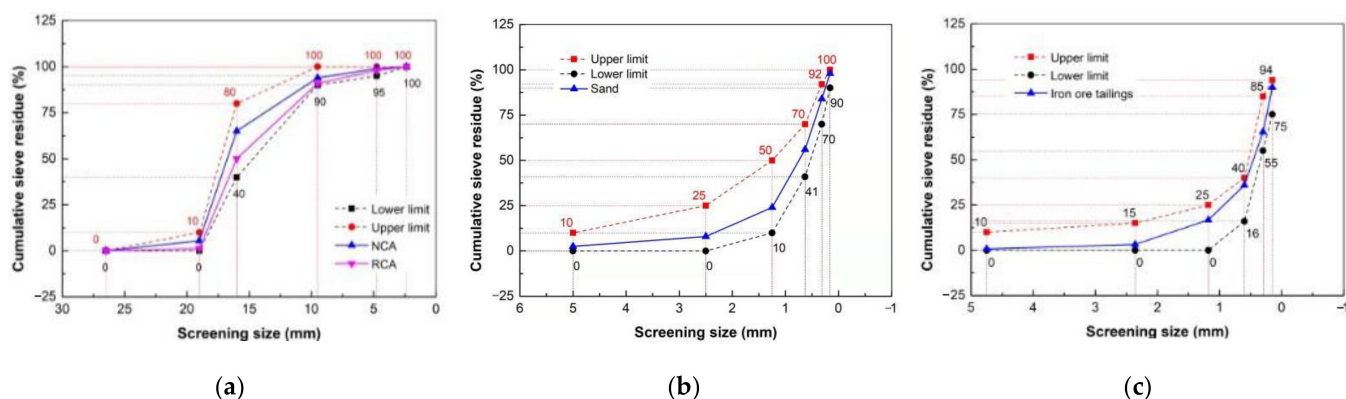

(a)   (b)   (c)

Figure 1. The grain gradation of coarse and fine aggregate: (**a**) coarse aggregate; (**b**) fine aggregate; (**c**) IOT.

Table 1. The main components of the cement and IOT.

Mineral Composition	C	O	Mg	Al	Si	S	K	Ca	Fe	Ti
Cement	4.12	47.54	0.74	1.54	6.11	1.10	0.53	56.84	0.93	0.01
IOT	0	56.49	6.95	8.38	17.46	-	3.02	1.68	5.28	0.74

Table 2. The main performance index of the cement.

Water Requirement of Normal Consistency (%)	Initial Setting Time (min)	Final Setting Time (min)	Fineness (45 μm)	Stability	Flexural Strength (MPa)		Compressive Strength (MPa)	
					3 d	28 d	3 d	28 d
28	160	280	2.8	Qualified	5.2	6.8	19.5	42.2

At the same time, based on previous results obtained by the research group, the replacement rate of recycled aggregate was 30% [18–22]. For the convenience of comparative analysis, the tailings dosage was 0%, 10%, 20%, 30%, 40%, 50%, 70% and 100% and the water–cement ratio and the sand ratio were 0.4 and 0.35, respectively. The mix proportion

was also carried out according to JGJ/T443-2018 [25]. The mix proportion of each test is shown in Table 4.

Table 3. The performance index of the main materials.

Performance Index	Apparent Density (kg/m³)	Bulk Density (kg/m³)	Crushing Value Index (%)	Water Absorption (%)	Sediment Percentage (%)	Moisture Content (%)	Organic Matter Content	Alkali Aggregate Reaction
NCA	2941	1749	10.3	1.33	0.72	0.8	Qualified	Qualified
RCA	2536	1467	14.8	7	1.86	3.02	Qualified	Qualified
Norm value [23]	≥2500	≥1300	≤16	-	≤1.0	-	Qualified	Qualified
Sand	2764	1830	12	2.12	1.2	4.1	Qualified	Qualified
IOT	2745	1824	19.53	8.7	2.9	1.45	Qualified	Qualified
Norm value [23]	-	-	≤10	-	≤3.0	-	Qualified	Qualified

Table 4. The mix design of the recycled concrete under different working conditions (kg/m³).

Serial Number	No	Cementitious Materials	Coarse Aggregate		Fine Aggregate		Water
		Cement	NCA	RCA	Sand	IOT	
1	NAC	538	1063	0	572	0	215
2	RAC-1	538	735	315	566	0	215
3	RAC-2	538	739	317	512	57	215
4	RAC-3	538	743	319	458	114	215
5	RAC-4	538	744	319	402	172	215
6	RAC-5	538	751	322	343	229	215
7	RAC-6	538	755	324	290	290	215
8	RAC-7	538	763	327	176	410	215
9	RAC-8	538	773	331	0	594	215

3. Test Setup

To simulate the chloride ion erosion characteristics of recycled concrete with tailings in salt spray environments, cube test blocks (100 mm × 100 mm × 100 mm) were used to test the salt spray erosion depth and change in ion content characteristics. To avoid the influence of multi-dimensional salt spray erosion on the erosion depth and ion concentration of the test block, a non-pouring surface was reserved as the salt spray erosion surface after the maintenance. The test process is shown in Figure 2.
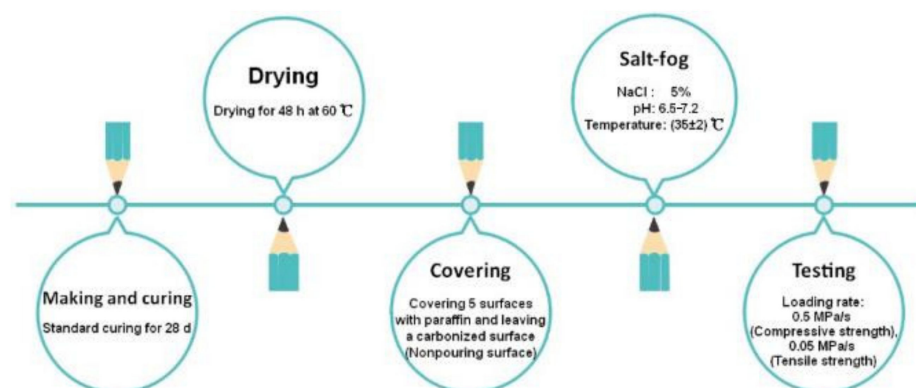

Figure 2. The salt spray test flow chart.

The test used a large salt spray erosion test box that was produced by Yingbai Technology Co., Ltd. in Wuxi Wuxi City, Jiangsu Province, China. When the test block had eroded to the specified age (7 d, 14 d, 28 d and 90 d), the salt spray erosion depth and ion content were measured using the following procedures:

(1) For the erosion depth measurement, a split along the erosion surface was sprayed with a 0.1 mol/L AgNO$_3$ solution and after 15 min, 10 points on the cleavage surface were measured with a digital depth meter and the average value was calculated;

(2) For the ion concentration value, the single side grinding method was used to collect powder from the eroded surface every 2 mm, layer by layer up to 10 mm. Then, holes were drilled every 5 mm to collect the powder and the powder was then filtered through a 0.16 mm sieve. According to the specifications [26], the total chloride ion concentration C_t and the free chloride ion concentration C_f were then extracted with dilute nitric acid mixed with distilled water and titrated potassium thiocyanate mixed with potassium chromate, respectively. The solid–liquid extraction method [27] was used to determine the mass fraction.

4. Test Results

4.1. Slump Values

Table 5 shows the slump values of the RAC with different IOT contents. It can be seen that the values decreased significantly with the increase in IOT content. When the content reached 100%, its value was 48.2% lower than that of NAC. The main reason for this is that the IOT had fine particles and a large specific surface area, which meant that its active components could promote the hydration of cement and then reduce the amount of free water and slump.

Table 5. The slump values of RAC with IOT.

No.	NAC	RAC-1	RAC-2	RAC-3	RAC-4	RAC-5	RAC-6	RAC-7	RAC-8
Cement	141	134	122	108	103	95	81	76	73

4.2. Compressive Strength

Figure 3 shows the change curve of the compressive strength of the cubes and its growth coefficient after salt spray erosion. The growth coefficient was defined as the ratio between the actual strength and the strength for the same age of salt spray erosion at 0 days (natural curing for 28 days). It can be seen from Figure 3a that the influence trends of the different tailings dosage conditions for the same erosion age were the same. Except for ordinary concrete, the compressive strength increased when the tailings content was lower ($\leq$40%) for the same salt spray erosion age and the higher the tailings content, the greater the compressive strength. For example, when the content of IOT increased from 0% to 40%, the compressive strength increased by 24.52% (0 d), 21.72% (7 d), 18.86% (14 d), 18.82% (28 d) and 19.60% (90 d). The main reason for this is that the tailings presented a certain fine powder and activity. Under the same conditions, the concrete became denser, the porosity decreased and the compressive strength increased with the addition of a 40% content of IOT. At the same time, when the IOT content was higher (>40%), the compressive strength decreased. This change trend was similar to that found in the results of other studies [27–29] on ordinary concrete.

Figure 3b shows the change rule for the compressive strength growth coefficient to salt spray erosion age under the same iron tailings mixture ratio. It can be seen that the change trends of the compressive strength growth coefficient caused by salt spray erosion were similar. With the same tailings content, the increase in erosion time generally demonstrated the trend of the growth coefficient of the compressive strength first increasing and then decreasing. Most of the concrete that was mixed with tailings had a peak point at 14 days, but the increased value was relatively limited with most being below 10% and some being less than 4%. In addition, there were a few concrete mixtures with peak points at 28 d, such as RAC-7 (70%) and RAC-8 (100%). The main reason for this is that when the tailings content was high, the design mix ratio of the concrete changed, the porosity increased and the peak point was pushed back. At the same time, when the salt spray erosion age

was 90 d, the tailings content was 100%. In this case, the compressive strength was also increased by 0.78% compared to 0 d.
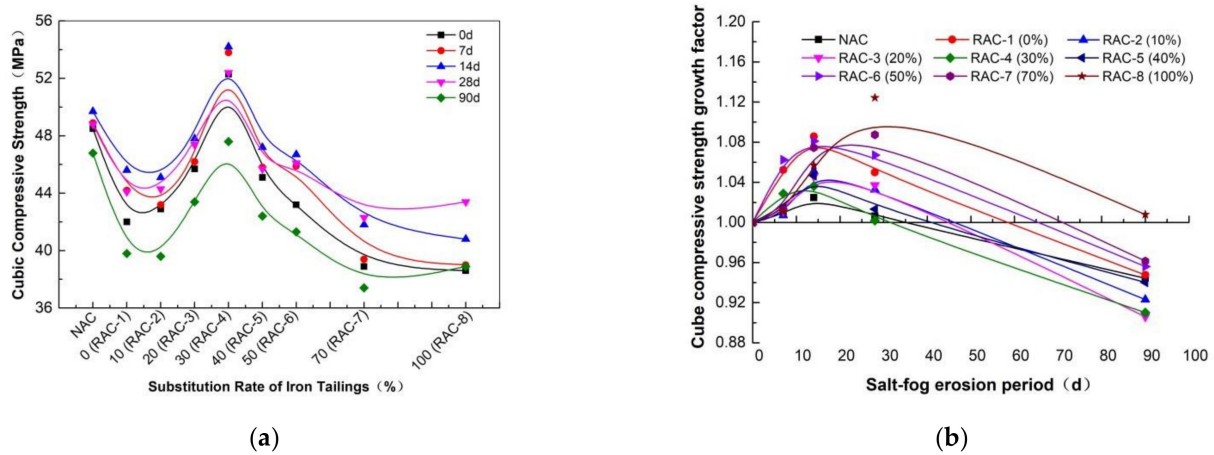

(**a**)   (**b**)

Figure 3. The influence of IOT content on the compressive strength of the cube: (**a**) the compressive strength value of the cubes; (**b**) the growth factor of the compressive strength of the cubes.

The above analysis showed that porosity was very significant in the salt spray erosion of concrete. Analyzing the reasons for this: on the one hand, the salt spray erosion products filled the pore structures and on the other hand, the salt crystals also had a swelling and densification effect on the pore structures [30]. Therefore, the greater the porosity, the more erosion products could accumulate and the less destructive the effect of erosion on the concrete.

4.3. Splitting Tensile Strength

Figure 4 shows the change curve between the splitting tensile strength of the recycled concrete cubes with different tailings contents and their corresponding growth coefficients under salt spray erosion.
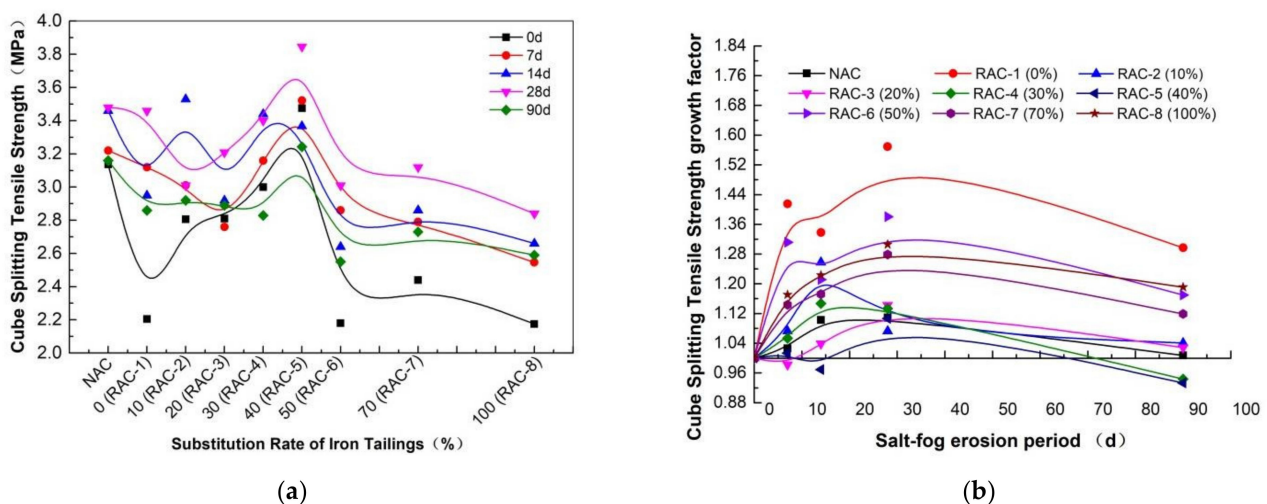

(**a**)   (**b**)

Figure 4. The influence of IOT content on the splitting tensile strength of the cubes: (**a**) the splitting tensile strength of the cubes; (**b**) the growth coefficient of the splitting tensile strength of the cubes.

Due to the low splitting tensile strength of the cubes, which was greatly influenced by human, mechanical and material factors, the value of the splitting tensile strength fluctuated to varying degrees; however, on the whole, when the content of tailings was low (≤40%), the splitting tensile strength values for different erosion ages showed an undulating trend with the peak point appearing when the content of tailings was 30–40%.

When the peak point was passed, the IOT content increased rapidly and then tended to level off. Most results showed that before 28 days of erosion, the value of splitting tensile strength gradually increased as the salt crystallization effect of the erosion increased, but then gradually decreased. The splitting tensile strength values at 90 days were even lower than those at 7 days, which showed that with the gradual increase in crystalline salt during those periods, a large expansion stress was generated in the cracks and pores and the tensile strength values were reduced accordingly.

Figure 4b shows the increasing growth coefficient of splitting tensile strength with the increase in erosion age with the same tailings content. Compared to the growth coefficient of salt spray of the compressive strength of the cubes, erosion age had less of an effect on splitting tensile strength and the intuitive phenomenon was that the slope of the curve was relatively small. On the whole, the growth coefficient for the same tailings content occurred after salt spray erosion for 14 to 28 days. Similar to the growth coefficient of compressive strength, the maximum value of the growth coefficient for splitting tensile strength occurred at 28 d for the condition of increased porosity, such as with RAC-1, RAC-7 (70%) and RAC-8 (100%). The growth coefficient at the peak point was also greater than that of compressive strength. For example, the splitting tensile strength growth coefficient of RAC-21, RAC-6 (60%) and RAC-8 (100%) increased by 56.9%, 38.1% and 22.3%, respectively, at the maximum point.

5. Erosion Depth

Figure 5 shows the erosion depth of the recycled concrete at different ages. It can be seen that the salt spray resistance of recycled concrete (RAC-1) was much lower than that of ordinary concrete (NAC) at the same erosion age. With the increase in IOT content, the salt spray erosion depth presented an approximate trend of first decreasing and then increasing, but the change trends were different. Approximately, when the tailings content was 30–40%, the erosion depth reached its minimum value. For example, after 90 days of salt spray erosion, the erosion depth of RAC-1 was 10.07% higher than that of NAC and the erosion depth of RAC-5 (u_{IOT} = 40%) was 14.29% lower than that of RAC-1 (u_{IOT} = 0%), indicating that the effect of an appropriate IOT amount on salt spray erosion was relatively obvious. The main reason for this is that the porosity of RAC was high and there were many interfacial transition zones, so salt spray could penetrate into the concrete more easily. As mineral admixtures, IOT particles are fine and have an obvious filling effect and activity, meaning that an appropriate amount could effectively promote the secondary hydration of cement particles and improve the pore structures and the compactness of the concrete matrix structures. As IOT replaced the fine aggregate in concrete, when the tailings content was too high, the optimal mix proportion of the concrete aggregate was, which led to an increase in the porosity of the concrete and a reduction in its anti-erosion ability.
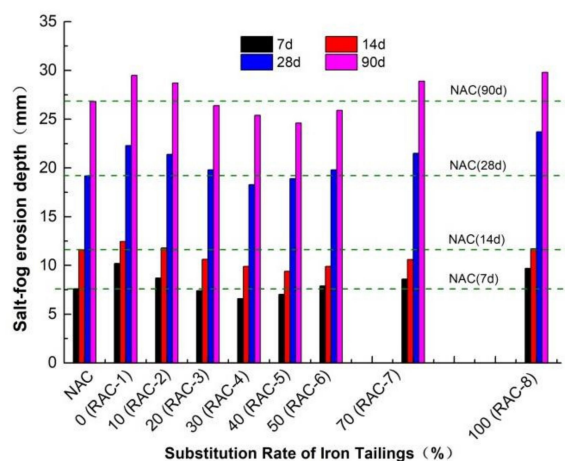

Figure 5. The effect of different IOT contents on the salt spray erosion depth of RAC.

6. Curing Ability of Chloride Ions

The absorption and curing effect of the chloride ions on concrete can greatly reduce the concentrations of free chloride ions and total chloride ions and the transmission rate of chloride ions, thereby reducing the risk of steel corrosion. Therefore, it was necessary to study the relationship between these three factors.

Mohammed [31] conducted a chloride ion erosion test on different cement types, cement components and concrete mixed with mineral powder, steel slag and other admixtures. It was found that the free chloride ion and total chloride ion contents conformed to the following formula:

$$C_t = K \cdot C_f \tag{1}$$

where K is the curing coefficient of concrete with different material types. The larger the K value, the stronger the curing ability of the concrete. In view of the diversity of cement varieties and cement components, this value is usually obtained by fitting the test results and reference [32] also used this model. However, some scholars [33] found that this model was not comprehensive and that it had a higher correlation when expressed as a complete linear model, i.e.:

$$C_t = K_1 \cdot C_f + K_2 \tag{2}$$

where K_1 is the influence coefficient and K_2 is a constant for the amount of total chloride ions that can be solidified and absorbed per unit mass of concrete, i.e., the amount of combined chloride ions when the free chloride ion content is 0. In our tests, Equation (2) was used to analyze the test results. In view of the small erosion depth and relatively few test data points in the early stages of the test (7 d and 14 d), the correlation between the free chloride ion and total chloride ion contents at 28 d and 90 d was studied in order to improve the accuracy of the study, as shown in Figure 6.
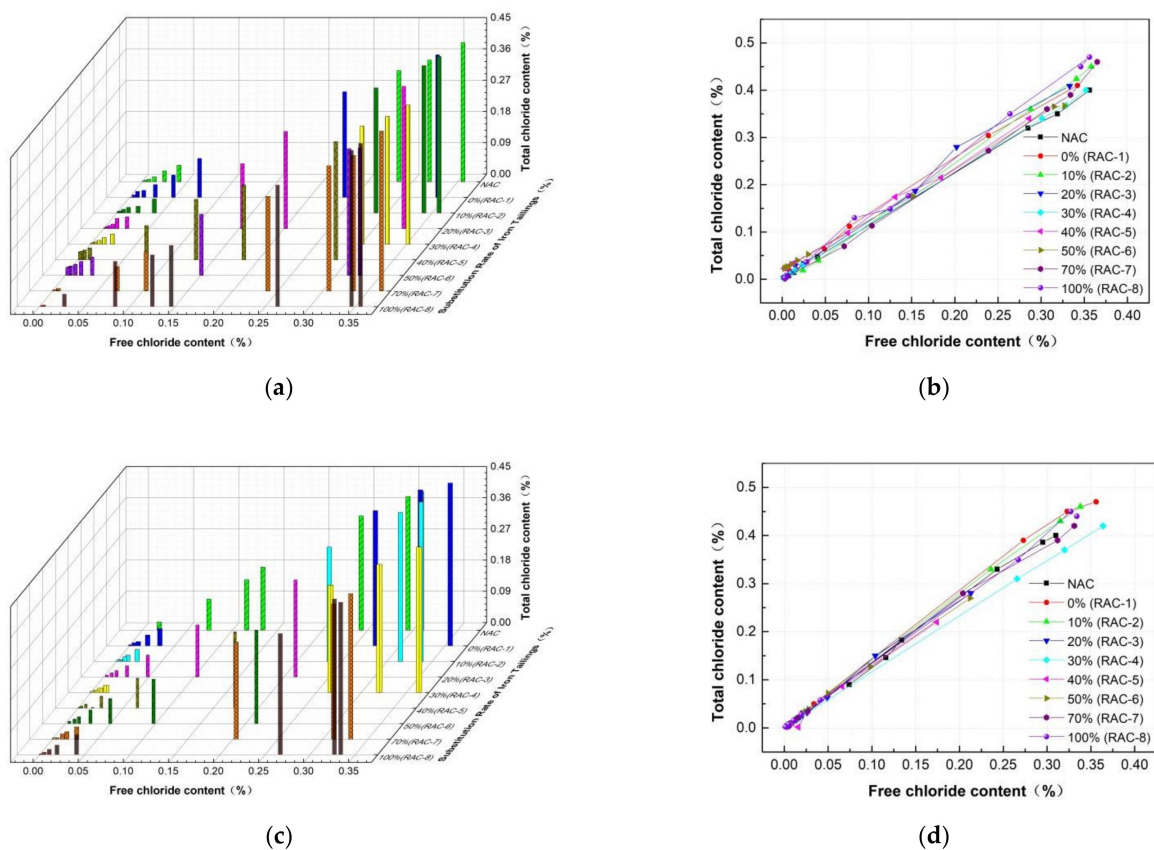

Figure 6. The relationship between C_t and C_f with different tailings dosages: (**a**) three-dimensional drawing (28 d); (**b**) plane figure (28 d); (**c**) three-dimensional drawing (90 d); (**d**) plane figure (90 d).

Figure 6a,c shows the location and size relationships of numerical points at the relevant erosion ages (28 d and 90 d), while Figure 6b,d represents the direct ratio relationships. Due to the low content of chloride ions, the position of powder collection and the density and permeability of the concrete had a great influence on the calculated chloride ion content. Compared to Figure 6a,c, the numerical points at the two erosion ages were in an approximately random distribution; however, it can be seen that the value of $C_f > 0.35\%$ when the figure was decreasing, indicating that the free chloride ion concentration (C_f) of concrete with the same tailings content gradually decreased with the increase in erosion time. As can be seen from Figure 6b,d, the ratio of free chloride ions to total chloride ions changed linearly (approximately and except for some scattered numerical points) and the curing coefficient K_1 changed very little. Figure 7 shows the change laws of the curing coefficients of different tailings content conditions at different erosion ages.
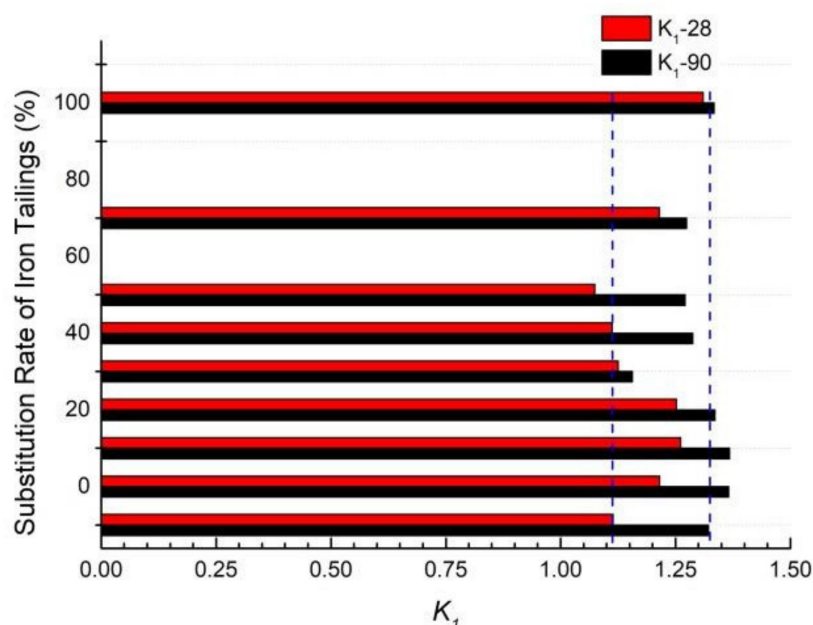

Figure 7. The comparative analysis of curing coefficients at 28 d and 90 d of salt spray erosion.

It can be seen that the curing coefficient increased with the increase in erosion age, which indicated that the curing ability of concrete gradually became stronger, i.e., more free chloride ions were converted into bound chloride ions. This was mainly because the longer the erosion time, the more calcium aluminate hydrate took part in the reaction and converted chloride ions into Friedel's salt and then, the corresponding bound chloride ion content increased. However, the increase degree was different for different IOT contents. When IOT content was 30%, 40% and 50%, the curing coefficient increased by 2.75%, 15.79% and 18.29%, respectively. The blue dotted line in the figure indicates the ratio of NAC at the corresponding erosion age. It can be seen that when the erosion age was small (28 d), the curing ability of the chloride ions was enhanced by high tailings content. When the erosion age higher (90 d), the alkali content of the concrete was reduced due to the tailings promoting the secondary hydration of concrete, which had an impact on the alkaline environment of Friedel's salt. Therefore, the curing performance of chloride ions decreased in the long term. However, due to the low activity of tailings, their impact on the alkaline environment of concrete was relatively limited. At the same time, the alkaline environment of RAC was stronger than that of NAC and the porosity of RAC was also higher, which caused the contact area with free chloride ions to be larger. Therefore, the improvement was relatively large in the short term, so the long-term curing ability would continue to increase.

7. Erosion Mechanisms

To explore the influence of IOT on the salt spray erosion resistance of RAC, an SEM analysis using the Hitachi S-4800 model at Chang'an University was carried out before and after the erosion took place and the degradation mechanisms were also studied.

Clusters of crystal products were formed at both 28 and 90 days of salt spray erosion. Under the same working conditions, the longer the erosion time, the more crystalline products were produced and the more obvious the cluster-like products were. Compared to the working conditions before erosion, the addition of RAC made the matrix structure relatively loose and also provided space for the formation, growth and development of chloride crystals. It was intuitively shown that the matrix structure of the concrete was covered by salt crystals due to the formation and physical expansion pressure of those salt crystals, meaning that the micro-cracks and harmful pores of the matrix structure were covered by salt crystals. At the same time, some connected fractures were gradually transformed into closed pores and harmful pores were further transformed into harmless pores. Meanwhile, when the erosion age was small, the mechanical properties and resistance to chlorine–salt erosion were slightly increased.

As shown in Figure 8b,d,f, when the erosion age was higher (90 d), it could be seen that the pores and micro-cracks of the concrete matrix structure were significantly higher than those at lower erosion ages (28 d), which showed that when the erosion time was longer, the concrete matrix structure was destroyed by the accumulation of salt crystalline substances. The reason for this is that, on the one hand, the physical expansion of the chloride crystals that accumulated in the pores caused tensile stress in the matrix structure and made it easy to crack. On the other hand, both cement hydration and the generation of chloride crystals needed to consume free water, which resulted in adverse effects on the matrix structure due to water migration as the amount of free water in the concrete was relatively small. To sum up, the mechanical properties and durability of almost all working conditions with high erosion ages decreased to varying degrees, which was similar to the results of Xue [34] and Yue [35].
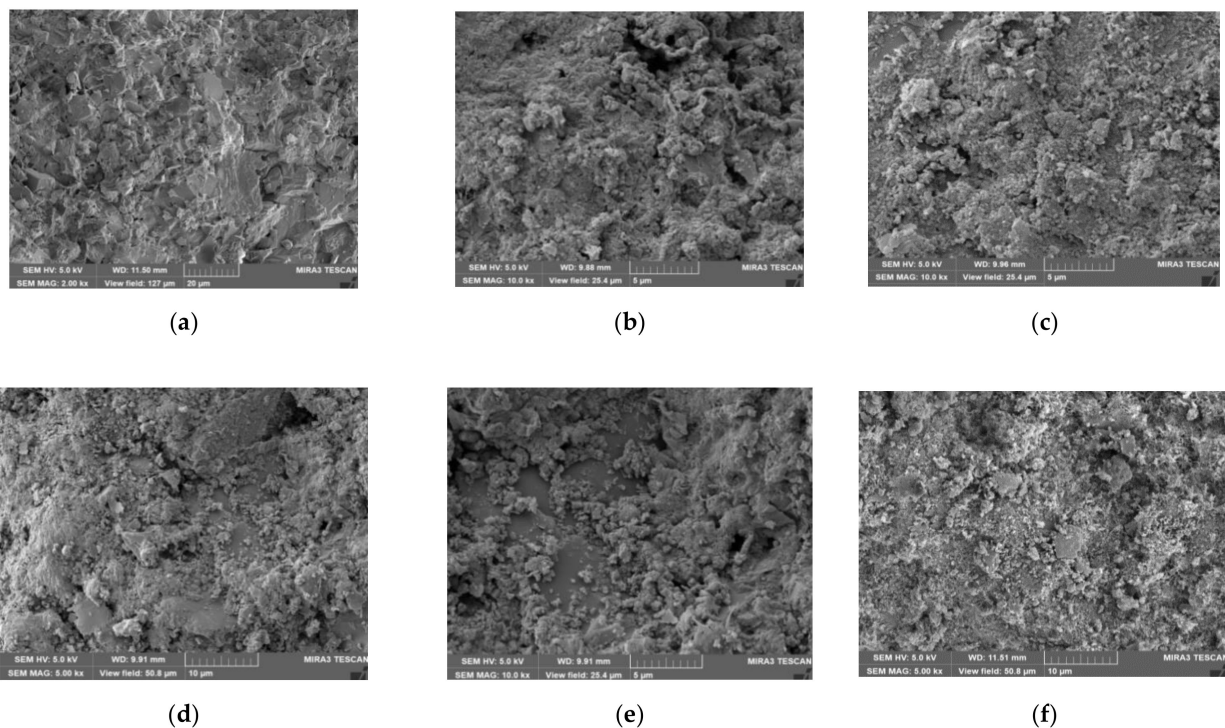

| (a) | (b) | (c) |

| (d) | (e) | (f) |

Figure 8. The scanning microscopic morphology of SEM images after different erosion cycles: (**a**) NAC (28 d); (**b**) NAC (90 d); (**c**) RAC (28 d); (**d**) RAC (90 d); (**e**) RAC-4 (28 d); (**f**) RAC-4 (90 d).

Combined with Figure 8d,f, Figure 9 shows the scanning microscopic morphology of SEM images of salt spray erosion on RAC with different tailings contents at 90 d.
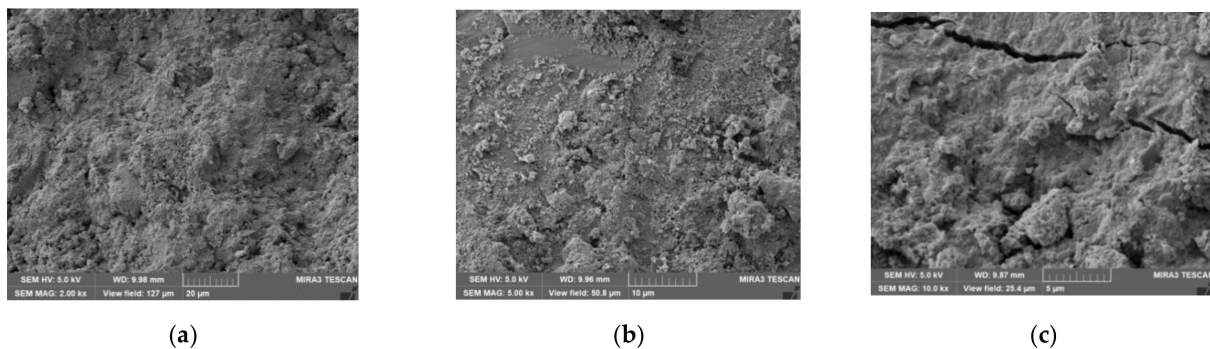

(**a**)   (**b**)   (**c**)

Figure 9. The scanning microscopic morphology of SEM images for different tailings contents after 90 d: (**a**) RAC-1; (**b**) RAC-5; (**c**) RAC-8.

Due to the introduction of recycled aggregate, when the IOT amount was small, a large number of pores appeared, as shown in Figures 8c and 9a. On the periphery of the pores, cluster-like crystal products, flocculent CSH and needle-like ettringite could be found. These three features intersected with each other within the pores and were embedded around the micro-pores. The concrete was refined, which effectively improved its porosity and pore structure and enhanced its resistance to chloride ion erosion. It can be seen from Figure 8b,e that there was still a small number of pores in the matrix structure, but they were relatively complete. As shown in Figure 9c, when the IOT content was high, a large number of micro-cracks and micro-pores were generated in the matrix structure, which greatly affected the integrity of the matrix structure and reduced its mechanical properties and erosion resistance, as shown in Figures 3a, 4a and 5. The main reason for this is that a small IOT content could promote hydration and fill pores, while excess additions changed the optimal mix proportion, increased porosity and caused the deterioration of each index.

8. Conclusions

In this paper, the mechanical properties, chloride ion concentration and chloride ion curing properties of recycled concrete with different IOT contents are analyzed at different salt spray ages (7 d, 14 d, 28 d and 90 d). The conclusions were as follows:

(1) At the same erosion age, when the content of iron tailings increased from 0% to 40%, the compressive strength of the concrete increased by 24.52% (0 d), 21.72% (7 d), 18.86% (14 d), 18.82% (28 d) and 19.60% (90 d), indicating that the higher the tailings content, the greater the compressive strength. However, when the tailings content was too high (>40%), it had the opposite effect. With the increase in erosion age, the compressive strength first increased and then decreased with a peak at 14–28 d. When the content of tailings was lower (≤40%), the splitting tensile strength increased and then decreased rapidly. The effect of erosion age on splitting tensile strength was less than that on compressive strength;

(2) The salt spray erosion resistance of RAC was much lower than that of NAC and when the IOT content was 30–40%, the salt spray erosion depth reached its lowest point;

(3) The higher the salt spray erosion age, the greater the corresponding growth coefficient. When the dosage of IOT was 30%, 40% and 50%, the curing coefficient at 90 d was 2.75%, 15.79% and 18.29% higher than that at 28 d, respectively. At the same erosion age, the ratio of free chloride ions to total chloride ions changed linearly and its curing coefficient K_1 first decreased and then increased, with the optimum IOT content being 30–50%;

(4) Through SEM microscopic morphology, it could be concluded that when the erosion age was low, the formation of salt crystals and the effect of physical expansion pres-

sure caused porosity to decrease. When the erosion age was higher, the cumulative expansion of crystals made them decrease in size. When added together, the crystallization and hydration products grew and developed in the micro-pores. When added excessively, the optimal mix ratio of the concrete changed, harmful pores and cracks were generated and resistance to salt spray erosion was reduced.

Author Contributions: Conceptualization, J.X. and S.W.; Data curation, T.L. and M.Z.; Formal analysis, J.X.; Investigation, M.Z.; X.C. and F.X.; Methodology, J.X.; Project administration, J.X.; Resources, J.X.; Software, T.L.; Supervision, J.X.; Validation, J.X.; Visualization, T.L., M.Z., X.C. and F.X.; Writing—original draft, J.X.; Writing—review & editing, T.L. All authors have read and agreed to the published version of the manuscript.

Institutional Review Board Statement: Not applicable.

Informed Consent Statement: Not applicable.

Conflicts of Interest: The authors declare no conflict of interest.

References

1. Figueiredo, R.; Brando, P.; Soutsos, M.; Henriques, A.B.; Mazzinghy, D.B. Producing sodium silicate powder from iron ore tailings for use as an activator in one-part geopolymer binders. *Mater. Lett.* **2021**, *288*, 129333. [CrossRef]
2. Kaplan, G.; Bayraktar, O.Y.; Gholampour, A.; Gencel, O.; Koksal, F.; Ozbakkaloglu, T. Mechanical and durability properties of steel fiber-reinforced concrete containing coarse recycled concrete aggregate. *Struct. Concr.* **2021**, *22*, 2791–2812. [CrossRef]
3. Nazarpour, H.; Jamali, M. Mechanical and freezing cycles properties of geopolymer concrete with recycled aggregate. *Struct. Concr.* **2020**, *21*, 1004–1012. [CrossRef]
4. Lv, X.D.; Liu, Z.A.; Zhu, Z.G.; Li, B.X. Study of the progress of tailings comprehensive utilization of raw materials in cement and concrete. *Mater. Rev.* **2018**, *32*, 452–456.
5. Liu, K.; Chen, Y.D.; Huang, D. Analysis on the research current situation and ruture trends of recycled concrete and analysis of future research trends. *Concrete* **2020**, *10*, 47–50. [CrossRef]
6. Jin, W.L.; Zhao, Y.X. *Durability of Concrete Structure*; Science Press: Beijing, China, 2014.
7. Kamiharako, A.; Tomiyama, J.; Arai, K. Estimation of the Amount of Chloride Ingress in Concrete Taking into Account Differences in the Amount of Adhering Salt on Bridge Members. *Concr. J.* **2016**, *54*, 164–169. [CrossRef]
8. Ronald, C.; Katsuchi, H.; Yamada, H.; Sasaki, H. Study on estimation of amount of airborne sea salt around bridge deck. *Kozo Kogaku Ronbunshu A* **2012**, *58*, 528–541. [CrossRef]
9. Mohamed, O.; Kewalramani, M.; Ati, M.; Hawat, W.A. Application of ann for prediction of chloride penetration resistance and concrete compressive strength. *Materialia* **2021**, *17*, 101123. [CrossRef]
10. Ariyachandra, E.; Peethamparan, S.; Patel, S.; Orlov, A. Chloride diffusion and binding in concrete containing NO_2 sequestered recycled concrete aggregates (nrcas). *Constr. Build. Mater.* **2021**, *291*, 123328. [CrossRef]
11. Rajamallu, C.; Reddy, T.C.; Arunakanthi, E. Service life prediction of self-compacted concretes with respect to chloride ion penetration. *Mater. Today Proc.* **2021**, *46*, 677–681. [CrossRef]
12. Su, L.W.; Cai, J.; Liu, P.H. Experimental Investigation in to RC Beam under the Action of Alternating Load in Salt-Spray Environment. *J. South China Univ. Technol.* **2017**, *45*, 97–104. [CrossRef]
13. Oritola, S.F.; Saleh, A.L.; Sam, A. Characterization of iron ore tailings as fine aggregate. *ACI Mater. J.* **2020**, *117*, 125–134. [CrossRef]
14. Protasio, F.; Avillez, R.; Letichevsky, S. The use of iron ore tailings obtained from the germano dam in the production of a sustainable concrete. *J. Clean. Prod.* **2020**, *278*, 123929. [CrossRef]
15. Wang, P.P.; Hu, J.L.; Yang, X. Study on the Strength of Recycled Concrete with Building Waste Mixed with Iron Tailings. *J. Hebei Inst. Archit. Civ. Eng.* **2019**, *37*, 38–42. [CrossRef]
16. Wei, T.; Quan, X.Y.; Yan, Q.Q. Experimental study on mechanical properties of recycled concrete with high ductility iron tailings. *China Concr. Cem. Prod.* **2019**, *8*, 93–96. [CrossRef]
17. Cui, H.H.; Yang, X.; Hu, J.L. Study on the matching and mechanical properties of regenerated concrete with iron tailings. *Sichuan Build. Sci.* **2018**, *44*, 100–105. [CrossRef]
18. Li, T.; Wang, S.; Xu, F.; Meng, X.; Li, B.; Zhan, M. Study of the basic mechanical properties and degradation mechanism of recycled concrete with tailings before and after carbonation. *J. Clean. Prod.* **2020**, *259*, 120923. [CrossRef]

19. Xu, F.; Wang, S.; Li, T.; Liu, B.; Li, B.; Zhou, Y. Mechanical properties and pore structure of recycled aggregate concrete made with iron ore tailings and polypropylene fibers. *J. Build. Eng.* **2021**, *33*, 101572. [CrossRef]
20. Tong, X.; Wang, S.L. Mechanical properties and microstructure analysis of recycled aggregate concrete with iron tailings. *Concrete* **2021**, *1*, 91–97. [CrossRef]
21. Xu, F.; Wang, S.; Li, T.; Liu, B.; Zhao, N.; Liu, K. The mechanical properties and resistance against the coupled deterioration of sulfate attack and freeze-thaw cycles of tailing recycled aggregate concrete. *Constr. Build. Mater.* **2021**, *269*, 121273. [CrossRef]
22. Li, T.; Wang, S.; Xu, F.; Li, B.; Dang, B.; Zhan, M.; Wang, Z. Study on Carbonation Damage Constitutive Curve and Mircroscopic Damage Mechanism of Tailing Recycled Concrete. *J. Renew. Mater.* **2021**, *9*, 1413–1432. [CrossRef]
23. Ministry of Housing and Urban-Rural Construction of the People's Republic of China. *JGJ52-2006*; Standard for Technical Requirements and Test Method of Sand and Crushed Stone (or Gravel) for Ordinary Concrete. China Architecture & Building Press: Beijing, China, 2006.
24. Ministry of Housing and Urban-Rural Construction of the People's Republic of China. *JGJ63-2006*; Standard of Water for Concrete. China Architecture & Building Press: Beijing, China, 2006.
25. Ministry of Housing and Urban-Rural Construction of the People's Republic of China. *JGJ/T 443-2018*; Technical Standard for Recycled Concrete Structure. China Architecture & Building Press: Beijing, China, 2018.
26. Ministry of Transport of the People's Republic of China. *JTS/T236-2019*; Technical Specification for Concrete Testing of Port and Waterway Engineering. China Communications Press: Beijing, China, 2019.
27. Choi, S.J.; Kim, Y.U.; Oh, T.G.; Cho, B.S. Compressive strength, chloride ion penetrability, and carbonation characteristic of concrete with mixed slag aggregate. *Materials* **2020**, *13*, 940. [CrossRef] [PubMed]
28. Gehlot, T.; Sankhla, S.S.; Parihar, S. Compressive strength and chloride ion permeability test of concrete incorporating fly ash and ggbs with diverse water binder ratio. *Mater. Sci. Forum* **2021**, *1*, 789. [CrossRef]
29. Ge, Y.F. *Fine Numerical Simulation and Experimental Study of Chloride Corrosion of Self-Compacting Concrete*; Southeast University: Nanjing, China, 2017.
30. Mousavinejad, S.; Sammak, M. Strength and chloride ion penetration resistance of ultra-high-performance fiber reinforced geopolymer concrete. *Structures* **2021**, *32*, 1420–1427. [CrossRef]
31. Mohammed, T.U.; Hamada, H. Relationship between free chloride and total chloride contents in concrete. *Cem. Concr. Res.* **2003**, *33*, 1487–1490. [CrossRef]
32. Wang, Y.; Liu, C.; Tan, Y.; Wang, Y.; Li, Q. Chloride binding capacity of green concrete mixed with fly ash or coal gangue in the marine environment. *Constr. Build. Mater.* **2020**, *242*, 118006. [CrossRef]
33. Zeng, J.J.; Fan, Z.H.; Xiong, J.B. Research on Durability of Metakaolin Concrete Based on Long-Term Exposure Experiment at In-Situ Marine Splash Zone. *J. South. China Univ. Technol.* **2018**, *46*, 53–60. [CrossRef]
34. Pillay, D.L.; Olalusi, O.B.; Awoyera, P.O.; Rondon, C.; Kolawole, J.T. A review of the engineering properties of metakaolin based concrete: Towards combatting chloride attack in coastal/marine structures. *Adv. Civ. Eng.* **2020**, *2020*, 8880974. [CrossRef]
35. Yue, J. *Study on Carbonation and Chloride Resistance of Autoclaved Nano-Modified Concrete*; China Mining University: Xuzhou, China, 2019.